Jestr

Journal of Engineering Science and Technology Review 15 (1) (2022) 168 - 176

JOURNAL OF
Engineering Science and Technology Review

Research Article

www.jestr.org

New Testing Device for the Grouting Reinforcement Performance of Fractured Rocks

Qinjie Liu[1,2], Benniu Wu[1,2,3,*], Qiang Fu [2,3] , Qiang Chen[3] and Feiyue Liu[4]

[1]*Joint National-Local Engineering Research Centre for Safe and Precise Coal Mining，Anhui University of science & technology, Anhui, Huainan, 232001, China*
[2]*Institute of Energy, Hefei Comprehensive National Science Center, Anhui, Hefei, 230031, China*
[3]*School of Mining Engineering, Anhui University of Science & Technology, Anhui, Huainan, 232001, China*
[4] *Department of Civil Engineering, McMaster University, Hamilton, Ontario L8S 4L7, Canada*

Received 22 February 2022; Accepted 1 April 2022

Abstract

In the existing studies on fractured rocks, specimens are prepared by using similar materials or rock fractures are prefabricated, and the weak parts of rock specimens themselves cannot be reflected. Grouting reinforcement tests fail to accurately simulate the influence of the weak plane characteristics of real joints in rocks breaking under a certain stress on the grouting reinforcement effect. However, the grouting effect can be evaluated by comparing the rupture energy of grouting specimens to solve the unreasonable grouting evaluation parameters. In this study, a new testing device for the grouting reinforcement performance of fractured rocks was designed. Multigroup grouting experiments were conducted on multiple real fractured rock specimens in accordance with different grouting parameters to explore the influences of primary rock strength, grouting material, and grouting pressure on the grouting effect. The grouting effect was evaluated by comparing the rupture energy before and after grouting. Results demonstrate that the improvement of postgrouting strength is positively correlated with the improvement of primary rock strength. The grouting effect was affected by the strength of grouting materials, that is, the higher strength of grouting materials contributed to more evident improvement of the mechanical properties of grouted rocks compared with those before grouting. When rocks with the same lithologies were grouted, a high grouting pressure promoted the bonding between slurry and rock fracture plane. The slurry was fully diffused in gaps to form a solid grouting body so that the overall stability of broken rock specimens was strengthened, and the consolidation surface of fracture plane was more stable. The proposed designed testing provides a good equipment to complete the grouting effect test and serves as a technical guide in field engineering.

Keywords: Fractured rock, grouting under pressure, mechanical property

1. Introduction

In rock engineering practice, the bearing state of fractured rock masses is common, especially surrounded rocks with broken soft rock roadways, chambers or working faces are encountered during deep mining, which fail to meet the practical engineering requirements [1]. Grouting reinforcement is an important means used to strengthen fractured rock masses and control engineering surrounding rocks [2]. Different grouting parameters and technological processes substantially change the interfacial characteristics and mechanical properties of grouting reinforcement bodies [3], thereby further affecting the comprehensive mechanical properties of fractured rock masses for grouting and the stability of engineering rock masses.

Grouting reinforcement of fractured soft rocks is a complex nonlinear process in material science, applied geology, rock mechanics, and engineering activities. Experiments are conducted by numerous scholars by using various means, and many methods, including filling of grouting materials in fractured rock masses [4], prefabrication of fractured rock specimens with rock-like materials [5], and prefabrication of injection holes and split fractures [6, 7], are proposed to explore the rock grouting effect. However, obvious deficiencies exist in the treatment of grouting reinforcement specimens. Specimens are manually prefabricated through various slurries by using universal building materials, such as macadam and stone for the test analysis. This process can only realize the performance test of rock-like materials containing random multiple fractures while failing to accurately describe the defects of engineering rocks themselves, such as joint fissures, accompanied by the noncompliance of test objects with practical engineering broken rock masses. The influences of weak planes, such as fractures and holes, on the grouting reinforcement effect are investigated by drilling holes, wire-electrode cutting or by other manual means of fracture prefabrication, which cannot reflect the weak parts of rock specimens. Consequently, grouting reinforcement experiments fail to accurately simulate the influence of the weak plane characteristics of real joints in rocks breaking under a certain stress on the grouting reinforcement effect.

A grouting reinforcement experimental method conforming to real fracture conditions of engineering broken rocks and a corresponding device must be developed. Real rock specimens must be used to explore the influences of different grouting parameters on the mechanical properties of grouting specimens, evaluate and analyze the grouting reinforcement effect, reveal the grouting reinforcement mechanism of broken rocks, and further optimize the grouting material parameters and technological processes. Therefore, promoting the application of broken grouting rocks will be of great theoretical importance and value in engineering.

*E-mail address: 18325775102@163.com
ISSN: 1791-2377
doi:10.25103/jestr.151.21

2. State-of-the-art

Rock fractures have been studied by many scholars through experiments, and grouting testing apparatuses have been developed. O.K. Mahabad et al. [8] proposed a numerical program based on discrete element combination for geomechanics. This program integrates the merits of continuous medium-based modeling method and discrete element method to overcome their deficiency, that is, they cannot capture the progressive damage and failure process in rocks. Sarfarazi V. et al. [9] explored the relationship between the point load and fracture toughness of granites through experiments and numerical simulations. Haeri H. et al. [10] studied the influence of cushion on the rock failure mechanism during direct shear test by using Particle Flow Code and investigated the shear fissures and tensile cracks in the model. Kirmaci A. et al. [11] analyzed the failure behavior of different types of rock specimens in uniaxial compressive strength tests through thermal imaging and characterized their energy dissipation profile through the temperature difference recorded by a thermal infrared imager during the experiment. Zheng F. et al. [12] presented an improved discontinuous deformation analysis program with a distribution key to analyze rock deformation and breakage. Van Eldert Jeroen et al. [13] explored the influences of grouting parameters on the grouting effect by using measurement while drilling index on the spot. Wang C. [14] evaluated the damage and failure mechanism of concentric porous granite under the action of the radial load through mechanical test, theoretical analysis, and numerical simulation. Fernando Jorne etal. [15] performed grouting by using porous media with different thickness values, verified the reliability of various empirical laws used to check the grouting injectivity, and detected different grouting permeation resistances generated by porous media to the flow through injection experiments. Milad Sangsefidi et al. [16] prefabricated defective rock specimens to explore the anticracking ability of differently sized defective rock specimens and proposed a method of directly determining the tangential stress component at the critical distance through finite element analysis.

Chen M. L. et al. [17] prefabricated fractured rock specimens through a high-pressure water jet system and studied the influence of rock fracture angle on the mechanical properties of rocks and their fracture evolution characteristics. Bi X. F. et al. [18] manually prefabricated rock cores with appropriate length and angle from the collected rock specimens by using a diamond microsaw and analyzed the influence of fractures on the mechanical behavior of salt rock . Huang Y. H. et al. [19] prefabricated rock specimens with two unparallel fractures by placing steel during the solidification of rock-like specimens and explored the failure behavior during the fracture initiation, expansion, and coalescence. Zhou T. et al. [20] prefabricated 3D embedded defects via 3D printing to investigate the mechanical behavior and volume fracture behavior of rock specimens. Le H. L. et al. [21] prepared specimens by prefabricating cement cubs, studied their performance changes under grouting conditions through mechanical tests, and stated that grouting improves the cohesion and frictional angle of rock specimens and enhances their strength. The above study results show that testing is the main factor influencing the grouting reinforcement of fractured rock masses and the most effective technical means of revealing the reinforcement mechanism.

In this study, a novel testing device for the grouting reinforcement performance of fractured rocks was developed on the basis of the existing experimental apparatus. Fractured rock specimens were simply grouted, and this device was verified by designing grouting experiments. First, uniaxial compression tests were performed for rock specimens to acquire fractured rock specimens and their mechanical parameters, followed by grouting reinforcement. Subsequently, the mechanical parameters were retested. Finally, the changes in their mechanical properties before and after grouting reinforcement were compared, so as to explore the influences of primary rock strength, grouting material strength, and grouting pressure on the grouting reinforcement effect, reveal the grouting reinforcement mechanism for fractured rock masses, and provide reference for evaluating the field grouting effect on surrounding rocks.

The remainder of this paper is organized as follows. Section 3 describes the grouting effect evaluation theory and the technical route of device development. Section 4 carried out the experimental verification of the device under different grouting parameters, as well as, the experimental results are analyzed. Conclusions are summarized in Section 5.

3. Methodology

3.1 Evaluation of grouting effect

The evaluation of grouting effect aims to measure the reasonability of grouting method, grouting materials, and grouting equipment. The evaluation indexes used are the failure mode of rock specimens and grouting strength, which are mainly correlated with postpeak rock performance [2, 22]. Li Z. et al. [23] studied the influences of normal stress, grouting thickness, and grouting strength on the shear strength of rocks before and after grouting. Wang Y. et al. [24] evaluated the grouting effect through the changes in the shear strength and effective cohesion before and after grouting. Alejano L.R. [25] indicated that the residual strength trend varies with rock type by studying the residual strength of granites. Therefore, the characterization of grouting effect only through the attenuation of mechanical parameters before and after grouting has certain limitations. The whole failure process should be considered when defining the strength of grouting reinforcement bodies rather than the prepeak or postpeak mechanical properties [26, 27].

For the description of grouting reinforcement effect on specimens, the stress–strain state is only a representative descriptive approach, which is a manifestation of the thermodynamic state of rocks from one aspect. The work made by loading to rocks leads to the changes in the stress–strain state of rocks, and a nonnegligible part of such work is dissipated, thereby resulting in changes in their damage state [28]. The evolution of this damage state affects the stress–strain state of rocks. Therefore, the stress–strain state of rocks is relatively complicated during their deformation and failure process, which is uncertain to some extent [29]. Simply taking the stress or strain as a failure criterion is inappropriate due to such uncertainties. Determining an accurate rock strength value is extremely difficult. In reality, rock failure is a state instability phenomenon driven by energy [30]. Therefore, if the energy transfer and transformation in the deformation and failure process of rocks can be analyzed in detail and a strength theory taking energy change as the failure criterion can be established, then the grouting laws of rocks can be accurately reflected

and the bearing capacity of grouting style can be better displayed by the energy changes.

Assume that the deformation and failure of rocks under the action of an external load are not accompanied by any heat loss. In accordance with the first law of thermodynamics, the relation among total energy W, dissipated energy W^d, and elastic energy W^e of rocks can be defined as follows:

$$W = W^d + W^e \tag{1}$$

The following equation can be obtained by processing the uniaxial compression test data of rock specimens.

$$\varepsilon_{ij} = \frac{d_{ij}}{D} \tag{2}$$

$$\sigma_{ij} = \frac{P_{ij}}{A} \tag{3}$$

where d_{ij} is the axial strain in the uniaxial compression process of specimens, mm;
D is the specimen length, mm;
A is the cross sectional area of specimens, mm^2.
P_{ij} is the load borne by specimens, kN;

$$W = \int \sigma_{ij} \mathrm{d}\varepsilon_{ij} \tag{4}$$

$$W^e = \frac{\sigma_{ij}^2}{2E} \tag{5}$$

$$W^d = W - W^e \tag{6}$$

where ε_{ij} is the strain during the uniaxial compressive deformation of rocks;
σ_{ij} denotes the stress during the uniaxial compressive deformation process of rocks, MPa.
E is the elasticity modulus of rocks.

The energy w absorbed by unit volume of rock specimen can be calculated as follows:

$$w = \frac{W}{V} = \frac{W^d + W^e}{V} = \frac{\int \sigma_{ij} \mathrm{d}\varepsilon_{ij}}{DA} \tag{7}$$

Hence, if the energy consumed to reach the instability failure of primary rock and the failure energy after grouting reinforcement can be experimentally determined and their relationship can be ascertained, then the influence of rock grouting on their energy state can be explained so as to evaluate the rock grouting effect. On this basis, grouting recovery coefficient Δ is defined, which is the ratio of rupture energy before grouting to that after grouting, that is,

$$\Delta = \frac{w_2}{w_1} \tag{8}$$

where w_1 and w_2 represent the energy absorbed by unit volume of rock specimen before and after grouting, respectively.

3.2 Development of testing device

3.2.1 Technical route

The technical route for designing this testing device for the grouting reinforcement performance of fractured rocks is displayed in Figure 1. First, a primary rock was taken as the study object to perform the uniaxial compressive first mechanics performance testing. Its original mechanical property parameters were recorded, and the stress–strain curves of the whole uniaxial compression process were acquired. Second, broken rock specimens were subjected to the grouting reinforcement experiment to obtain grouting-reinforced rock specimens. Third, the secondary uniaxial compressive mechanics performance testing was conducted for the reinforced specimens, and the mechanical property parameters were recorded. Finally, the data collected twice were compared to acquire the influences of specific conditions on the grouting reinforcement performance.

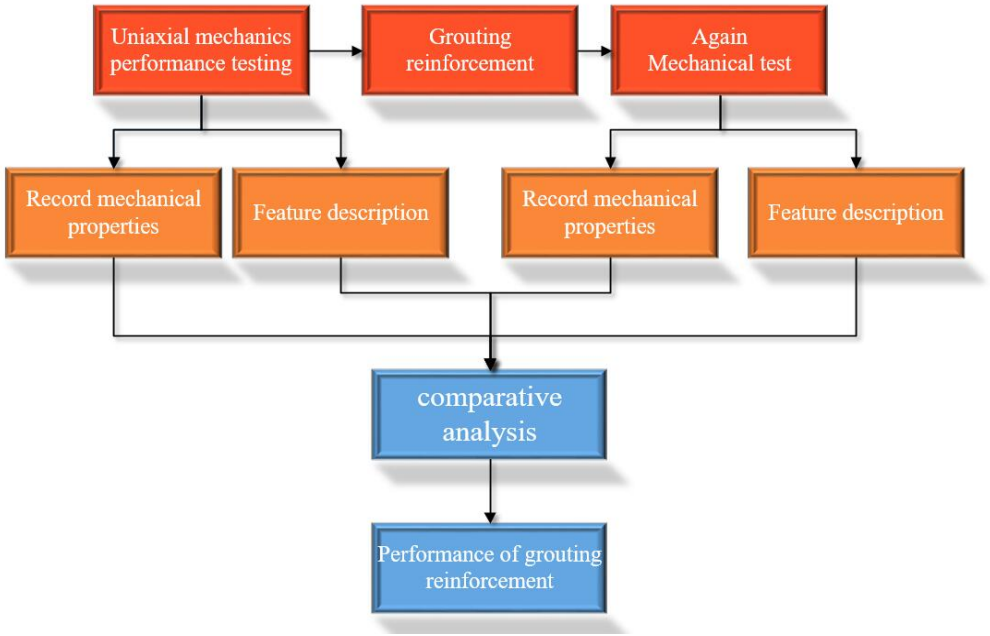

Fig. 1. Technical roadmap

3.2.2 Main equipment

The grouting reinforcement performance of fractured rocks was tested mainly through triple synchronous grouting device, rock testing system, and data acquisition system, with the structural diagram shown in Figure 2.

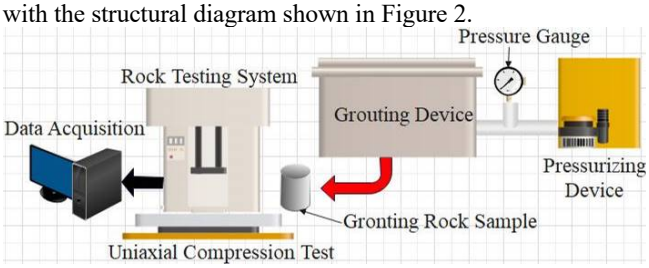

(a)

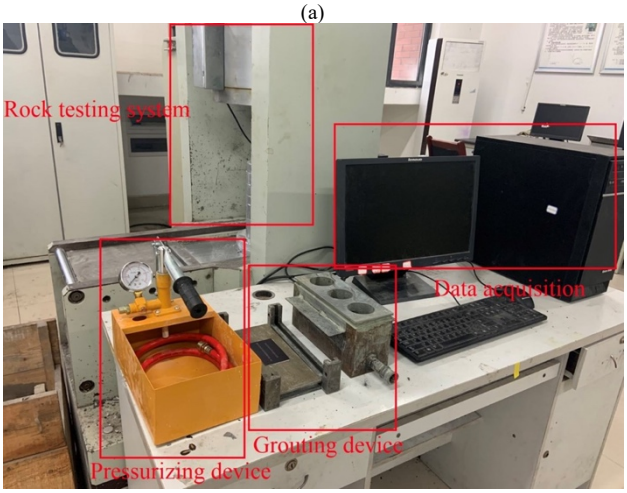

(b)

Fig. 2 Main equipmen. (a) System assembly drawing. (b) System structure

3.3 Development of triple synchronous grouting device

A triple synchronous grouting device was developed and designed for fractured rock specimens. This device [Figure 3 (a)] was used to grout fractured rock specimens on the basis of guaranteed gas tightness. The cavity of this device was designed into three circular cavities that can accommodate rock specimens (Φ50 mm×100 mm) to maintain the environment of three rock specimens during grouting. The three circular cavities were mutually connected via the upper and lower grout outlets and injection port.

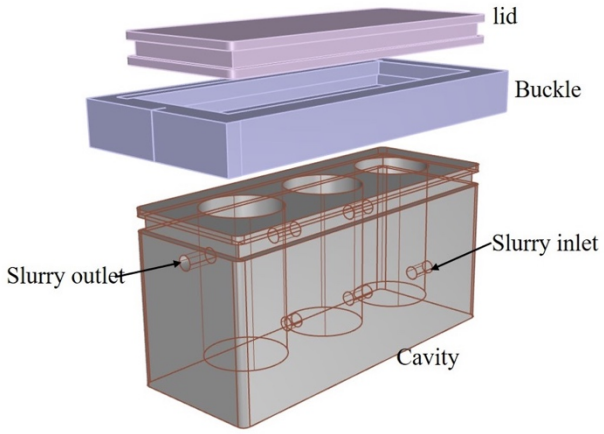

Fig. 3 Device diagram

Analog calculation of this device was performed through the finite element analysis method to determine its detailed design parameters. The model was made of 45# steel, and the material properties were defined as follows: tensile strength (600 MPa), yield strength (355 MPa), and density (7.85 g/cm^3). For the sake of convenient analysis, the pressure acting inside the cavities was simplified, and a pressure of 6 MPa was applied to the internal surface of cavities. The model was simulated by pressurization to obtain the model deformation, stress, and safety factor distribution nephograms (Figure 4). The maximum deformation, maximum equivalent stress, and minimum overall safety factor of grouting device were 3.526×10^{-3} mm, 56.29 MPa, and 6.39, respectively, which met the strength requirements during the use of this equipment. Thus, the equipment can be fabricated to conduct the experimental verification.

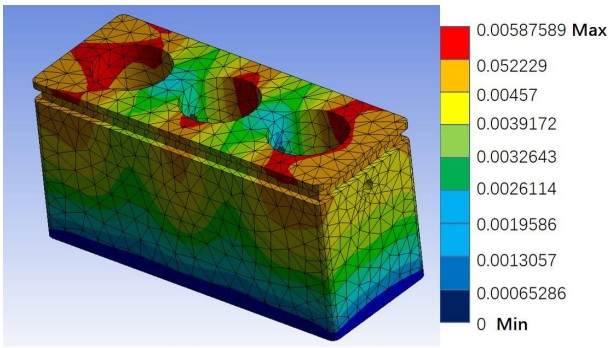

(a)

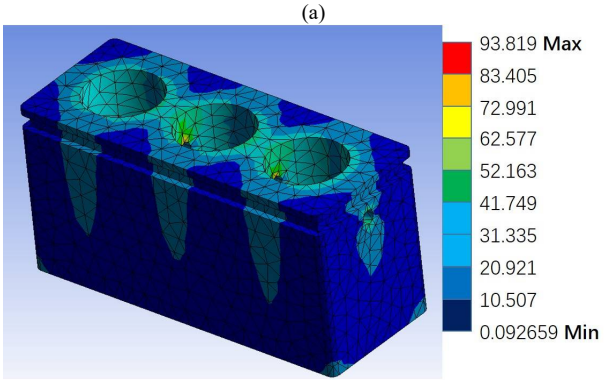

(b)

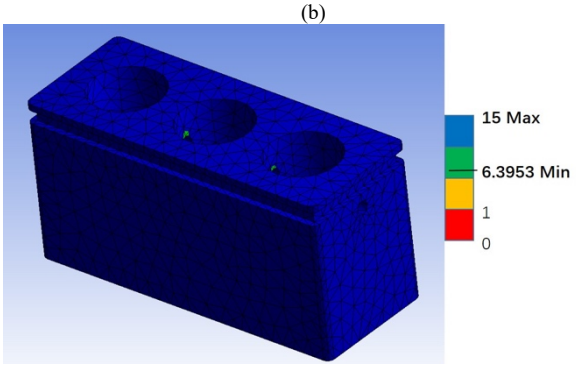

(c)

Fig. 4 Cloud diagram of grouting device deformation, equivalent stress, and safety factor.(a) Deformation nephogram. (b) Stress nephogram. (c) Safety factor cloud chart

4 Result analysis and discussion

4.1 Experimental schemes

The influence mechanism of grouting parameters on the grouting effect was analyzed on the basis of the grouting effect evaluation in Section 3.1. Three groups of tests were designed in this study to display the effect of the proposed testing device from different aspects (Table 1). In group A, the changes in the mechanical properties of specimens (A-1, A-2, and A-3) with the same lithology but different strength values before and after grouting were investigated. In group

B, the influences of grouting materials with different strength values (cements with different grades) on the grouting effect were explored, and the specimens were divided into three groups. In group C, the influence laws of different grouting pressures on the grouting effect were probed. In this case, the same grouting materials with the same lithology were selected and experimented. The specific grouping results of rock specimens are listed in Table 1.

Table 1. Grouping of rock specimens

No.	Lithology	Grouting material	Influence factor
A-1	Sandy mudstone	P·I 52.5 cement	Primary rock strength
A-2	Sandy mudstone	P·I 52.5 cement	
A-1	Sandy mudstone	P·I 52.5 cement	
B-1	Sandy mudstone	P·I 42.5 cement	Grouting material
B-2	Sandy mudstone	P·I 52.5 cement	
B-3	Sandy mudstone	P·I 62.5 cement	
C-1	Sandy mudstone	P·I 52.5 cement	Grouting pressure
C-2	Sandy mudstone	P·I 52.5 cement	
C-3	Sandy mudstone	P·I 52.5 cement	

4.2 Experimental steps

First, each rock specimen was subjected to the uniaxial compression test with continuous loading until reaching its complete failure, as shown in Figure 5 (a). The broken specimens were collected after the experiment. The axial force and axial deformation data and the stress–strain curves in the uniaxial compression process of rocks were acquired, and the fractured rock specimens were prepared.

Second, the fractured rock specimens were placed in the grouting device, as shown in Figure 5 (b). The grouting material was prepared at the water cement ratio of 1:1, followed by the grouting reinforcement of rock fractures [Figure 5 (d)]. Pressurization was manually performed by using a grouting pump until the slurry filled the grouting device. The grouting under pressure was continued by closing the grout outlet after the overflowing of slurry. Grouting was stopped after the pressure gauge reached the experimental design requirement. The testing device stood for 1 h , and the grouting specimens were taken out, placed in the shade to dry, and then cured for 48 h after the solidification.

Finally, the uniaxial compression test was performed on the grouting samples once again to comparatively analyze the two groups of data before and after grouting. On this basis, the grouting reinforcement effect was evaluated by combining the failure status of specimens. The above operations were repeated in accordance with the experimental design to prepare the next experiment.

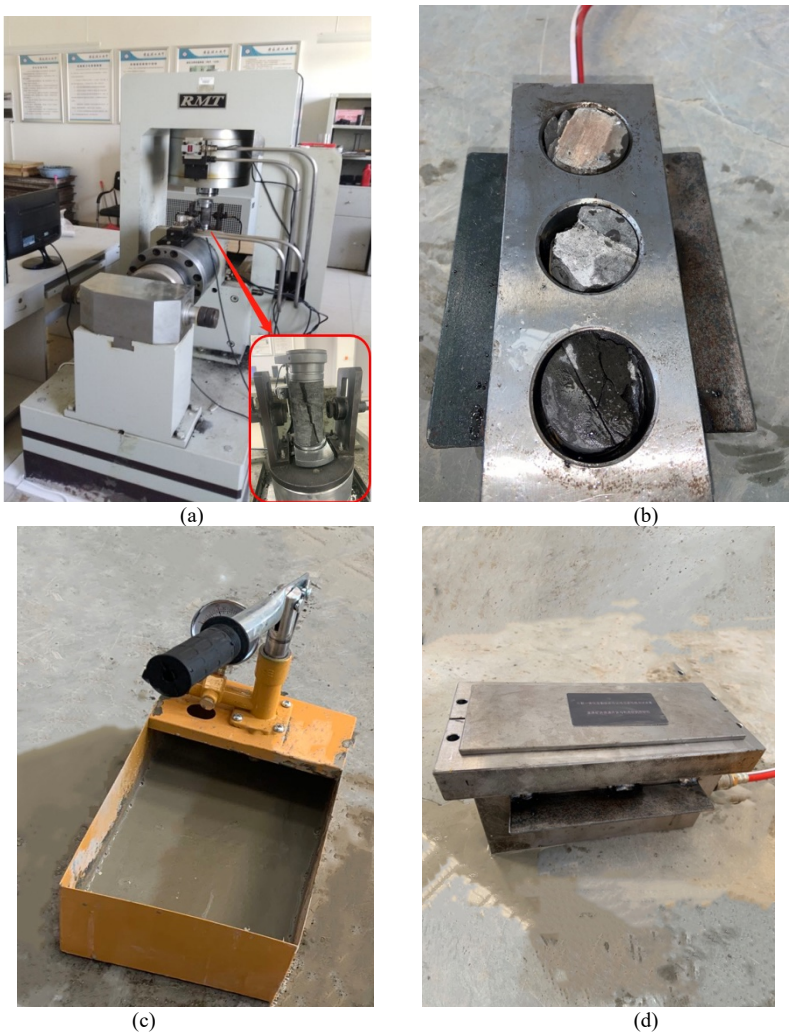

Fig. 5 Test procedure. (a) Uniaxial compression specimen. (b) Place grouting sample. (c) Slurry preparation. (d) Grouting reinforcement

4.3 Analysis of experimental results

4.3.1 Analysis of grouting effect under different lithologies

Under the pressure of 1 MPa, P·I 52.5 cement was used to perform the grouting reinforcement and testing of rock specimens with different lithologies to obtain the stress–strain relation curves (Figure 6) before and after grouting. The pregrouting curves were A-1, A-2, and A-3, and the postgrouting curves were A-1*, A-2*, and A-3*. The loading continued, and the stress dropped sharply, with evident brittle failure, after the rock specimens reached a peak stress before grouting. The stress–strain curves of specimens after grouting reinforcement were relatively gentle, being similar to those before grouting, and reached their peak values from the elastic stage, followed by the failure stage. The stress–strain curves of rock specimens under uniaxial compression were gentle, the peak stress was elevated in comparison to the residual strength of primary rocks, and the specific increase amplitude varied with the primary rock strength. The increase amplitude of grouting specimens with high primary rock strength was more evident than that of specimens with low primary rock strength.

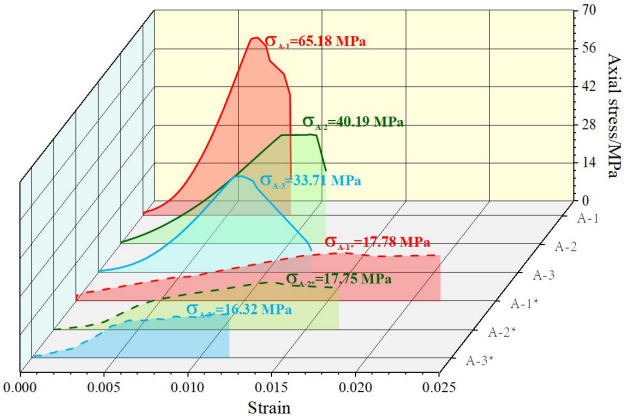

Fig. 6 Stress–strain curve of group A sample before and after grouting

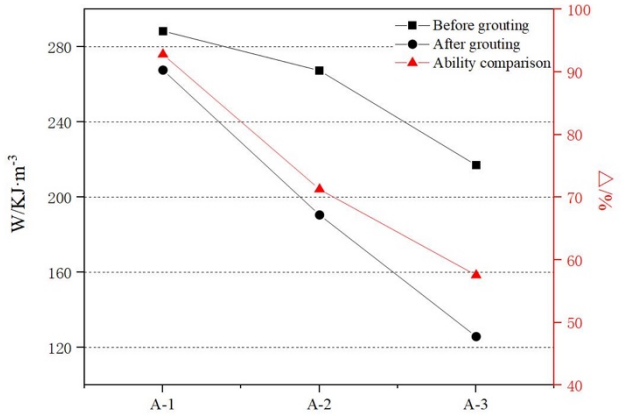

Fig. 7 Comparison of the Δ values of group A samples before and after grouting

The uniaxial compressive strength of three rock specimens (A-1, A-2, and A-3) gradually declined. The comparison results between postgrouting fracture energy and primary rock fracture energy are displayed in Figure 7. The pregrouting fracture energy and postgrouting fracture energy of specimens were compared, and the ratio of energy absorbed by rock specimens was 92.8%, 71.2%, and 57.8%. All specimens in this group were subjected to grouting reinforcement using the same material under the same pressure. Only the primary rocks had different strength values, which was the only factor causing the comparative difference among the three rock specimens in the fracture energy. Therefore, the specimens with high primary rock strength absorbed the same energy after grouting as that before grouting. With the improvement of primary rock strength, the postgrouting fracture energy increased, the stability of grouting reinforcement body was better, and the grouting effect was enhanced. On this basis, the strength of grouting reinforcement body can be effectively enhanced by grouting rock masses with great primary rock strength.

4.3.2 Analysis of grouting effect under different slurry conditions

Sandy mudstones with average uniaxial compressive strength of 29.7 MPa were selected as study objects. After the three specimens in group B were subjected to the mechanical property test, they were reinforced by grouting using P·I 42.5, P·I 52.5, and P·I 62.5 cements, respectively. The stress–strain curves acquired through the secondary mechanical property test are displayed in Figure 8. Group B-1 were specimens grouted with P·I 42.5 cement, group B-2 were those grouted with P·I 52.5 cement, group B-3 were those grouted with P·I 62.5 cement, and those carrying * were rock specimens after grouting reinforcement.

The stress–strain curves of grouting specimens had obvious compaction stage, elastic deformation stage, yield stage, and failure stage. However, they were obviously different due to the influence of grouting materials. The compaction stage was the running-in stage between rock block and grouting material. In this stage, the grouting interface inside each specimen experienced occlusion deformation after bearing a stress, and this stage was more apparent under lower grouting material strength and weaker bonding force. Each specimen started entering the elastic deformation period after compaction, during which the rock block and grouting material jointly bore the stress, and the compression resistance manifested by each specimen was their coupling result. With higher grouting material strength and better bonding performance, the duration of elastic stage was longer, and the linear slope was greater. With continuous pressurization, the stress concentration phenomenon was more obvious inside the specimen. Fracture deformation occurred inside the rock block, grouting material or on the cementation surface after the stress concentration reached a certain degree. Thus, the integrity of each specimen was damaged, and its nondeformability was weakened, followed by the yield stage. The fractures inside the specimen continuously developed, expanded, and led to the radical loss of its bearing capacity, and then the stress–strain curve entered the postpeak failure stage.

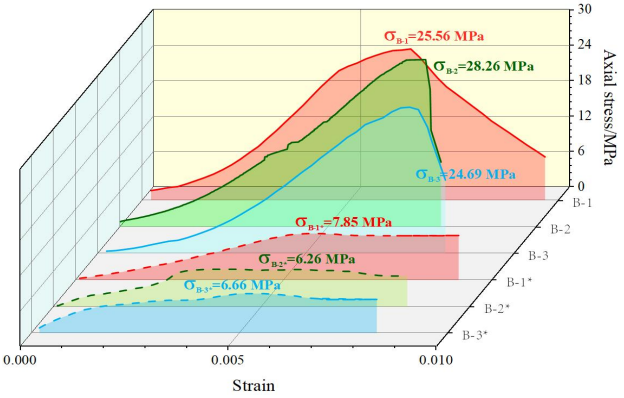

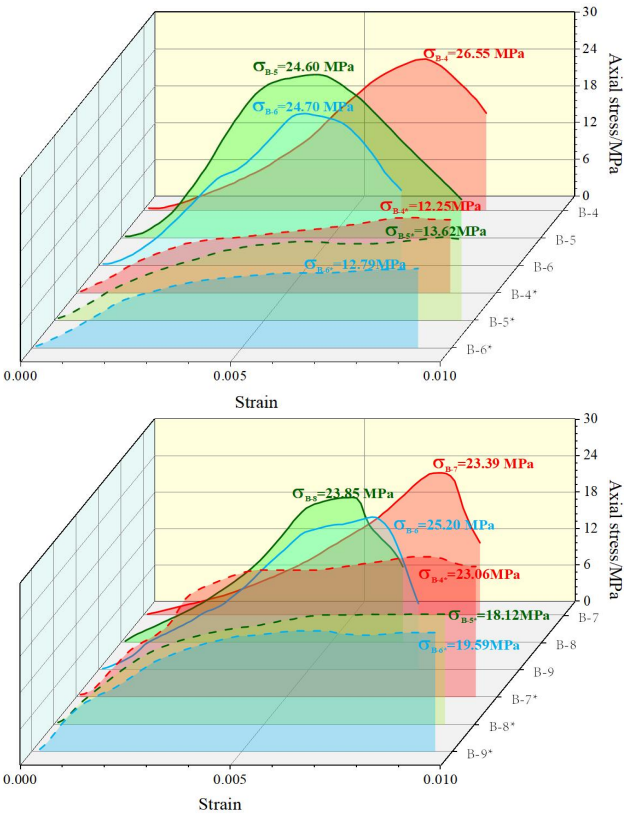

Fig. 8 Stress–strain curve of group B sample before and after grouting

The failure energy of each specimen in case of uniaxial compression failure was clearly acquired by processing the stress–strain curves before and after grouting (Table 2), and the failure energies of all specimens obtained through the three grouting experiments were linearly fitted (Figure 9). Under the pressure of 2 MPa, the values of specimens grouted with P·I 42.5 cement were 36.99%, 39.25%, and 46.36%, those specimens grouted with P·I 52.5 were 75.25%, 76.88%, and 86.33%, and those specimens grouted with P·I 62.5 cement were 197.37%, 150.79%, and 137.47%. This finding reflected that with the improvement of grouting material strength, the energy ratio per unit volume of each rock specimen before and after grouting increased, and the strength of grouting body was enhanced by improving the mechanical properties of grouting materials. A similar conclusion can be obtained from the fitted curves of energy comparison. Under the same lithology and grouting pressure, the rock specimens were grouted, with the effect mainly decided by the grouting material. Specifically, under higher material strength, the corresponding failure energy to be absorbed by grouting reinforcement body until a failure will be higher, and its compressive resistance will be better, so as the grouting effect.

Table 2. Fracture energy of specimens in Group B before and after grouting

No.	Cement No.	W_1 (KJ/m^{-3})	W_2 (KJ/m^{-3})	Δ
B-1	PI 42.5	132.93	49.17	36.99%
B-2	PI 42.5	102.99	40.42	39.25%
B-3	PI 42.5	92.11	42.70	46.36%
B-4	PI 52.5	102.21	76.92	75.25%
B-5	PI 52.5	126.81	97.50	76.88%
B-6	PI 52.5	102.65	88.63	86.33%
B-7	PI 62.5	83.32	164.45	197.37%
B-8	PI 62.5	86.57	130.53	150.79%
B-9	PI 62.5	108.27	148.84	137.47%

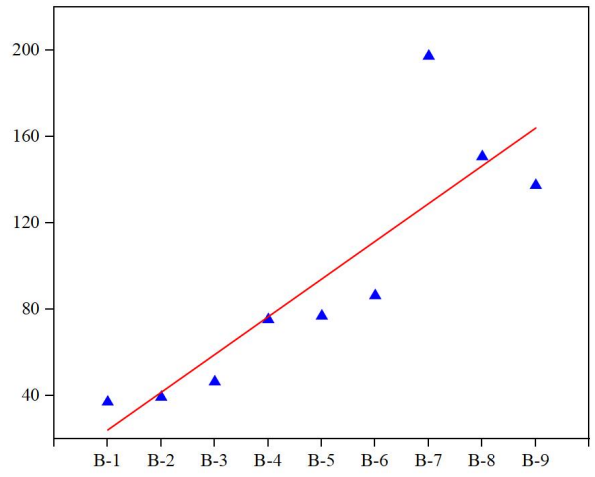

Fig. 9 Linear fitting of the Δ value of group B sample

4.3.3 Analysis of grouting effect under different grouting pressures

Three groups of experiments were designed to explore the influence of different grouting pressures on the rock grouting effect. All rock specimens used in the experiments were sandy mudstones with good homogeneity. The grouting reinforcement experiment was performed for rock specimens by using PI 52.5 cement under the grouting pressure of 0.5, 1.,0 and 2.0 MPa. The stress–strain curves of rock specimens before and after grouting were organized, as shown in Figure 10, in which the postgrouting curves carried *.

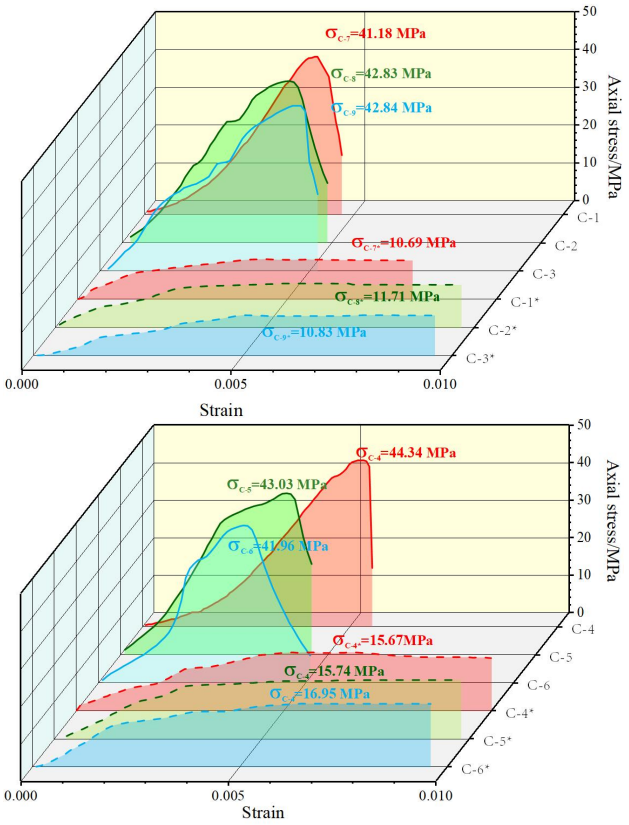

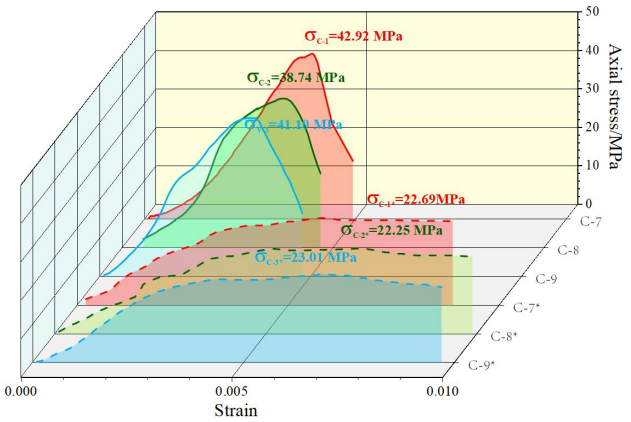

Fig. 10 Stress–strain curve of group C sample before and after grouting

The fracture energies of three specimens before and after grouting are listed in Table 3. Under the grouting pressure of 0.5 MPa, the ratio of energy adsorbed by unit volume of specimens after grouting was 77.56%, 78.49%, and 60.96%, those under 1 MPa was 117.62%, 104.12%, and 118.90%, and those under 2 MPa reached 155.30%, 171.62%, and 148.18%. From the linear fitting diagram (Figure 11) of energy comparison, the absorption energy per unit volume of grouting body was improved with the improvement of grouting material strength. With the increase in grouting pressure, the slurry was better diffused in rock gaps so as to better facilitate the bonding between slurry and broken rock mass and form a solid slurry body. On this basis, the overall stability of broken rock specimens was greatly enhanced, and the solidification surface of broken plane was more stable.

Table 3. Fracture energy of specimens in group B before and after grouting

No.	Grouting pressure (MPa)	W_1 (KJ/m^{-3})	W_2 (KJ/m^{-3})	Δ
C-1	0.5	90.95	70.54	77.56 %
C-2	0.5	120.28	94.41	78.49 %
C-3	0.5	128.83	78.54	60.96 %
C-4	1.0	105.45	124.03	117.62 %
C-5	1.0	119.48	124.40	104.12 %
C-6	1.0	107.79	128.16	118.90 %
C-7	2.0	98.96	153.65	155.30 %
C-8	2.0	98.42	168.94	171.62 %
C-9	2.0	114.75	170.04	148.18 %

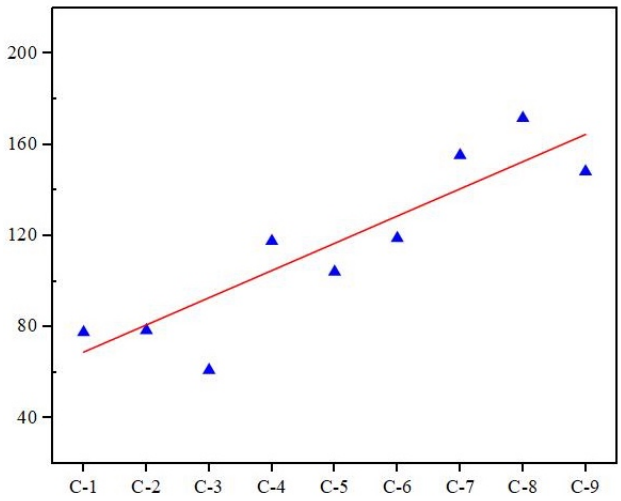

Fig. 11 Linear fitting of the Δ value of group C sample

5. Conclusions

Given that rock specimens are usually prepared by using similar simulation materials in rock fracture grouting experiments, a triple integrated testing device was designed for the grouting reinforcement performance of fractured rocks in this study. The testing device was fabricated after design and simulation, and was tested by using rock specimens. The failure energy of each specimen before and after grouting was comparatively analyzed. The conclusions are summarized as follows:

(1) The postgrouting fracture energy will be elevated with the enhancement of primary rock strength by comparing the fracture energy before and after grouting. Thus, the compressive strength of grouting specimens can be effectively enhanced by improving the rock strength.

(2) With higher grouting material strength, the mechanical properties of grouting reinforcement body become better, and its bearing capacity is strengthened, manifesting that the bearing capacity of grouting specimens can be effectively enhanced by the increase in slurry strength.

(3) The grouting effect is influenced by grouting pressure. Specifically, the fracture energy of grouting reinforcement bodies with the same grouting material and lithology is increased with the increase in the grouting pressure.

Thus, the designed testing device for the grouting reinforcement performance of fractured rocks has simple operation, and specimens can be collected and experimented on the field, which can facilitate to acquire the grouting effect in practical engineering. However, the specimen changes before and after grouting are comparatively analyzed in terms of energy in this study. The grouting effect is affected by the micro-level bonding state between the grouting material and broken plane of rock specimens. Therefore, this topic should be explored in the follow-up study to perfect the grouting reinforcement mechanism of the designed testing device.

Acknowledgements

The authors are grateful for the support provided by the Institute of Energy, Hefei Comprehensive National Science Center under Grant (No.21KZS215),Open Research Grant of Joint National-Local Engineering Research Centre for Safe and Precise Coal Mining (Grant NO.EC2021014) and Graduate innovation fund of Anhui University of technology in 2021 (2021CX2013).

References

1. Cao, R. H., Cao, P., Lin, H., Fa, X., Zhang, C. Y., Liu, T. Y., "Crack Initiation, Propagation, and Failure Characteristics of Jointed Rock or Rock-Like Specimens: A Review". *Advances in Civil Engineering,* PT.3, 2019, pp. 1-31.
2. Yu, X., Sun, Z., Deng, M., Xin, J.L., "Grouting Technique for Gob-Side Entry Retaining in Deep Mines". *Advances in Civil Engineering,* 8, 2021, pp. 1-9.
3. Li, Z., Liu, H., Dun, Z., Ren, L. W., Fang, J.J., "Grouting effect on rock fracture using shear and seepage assessment". *Construction and Building Materials,* 242, 2020, pp. 1-13.
4. Li, Z., Li, S., Liu, R., Jiang, Y.J., Ha, F., "Grouting reinforcement experiment for water-rich broken rock mass". *Chinese Journal of Rock Mechanics and Engineering,* 36(01), 2017, pp. 198-207.
5. Zhang, J. F., Xu, R. P., Liu, Y., Zhang, H, M., Qing, X.R., Chen, M., "Experimental study on mechanical properties of grouted fractured rock mass under freeze-thaw cycles". *Journal of Experimental Mechanics,* 36(03), 2021, pp. 378-388.
6. Guo, D. M., He, T. Y., Yang, R. S., Ye, S. D., Zhang, Y. Q., Li, X. P., "CT analysis on micro-cement grouting effect for fractured rock sample". *Journal of Mining & Safety Engineering* 34(05), 2017, pp. 987-992.
7. Liu, J., Li, Z., Yang, Y. N., Zhang, Z. R., Tang, H. Y., Gao, J., Shen, J., "Feasibility and experimental study of visualized seepage device of rock fracture". *Rock and Soil Mechanics*, 41(12), 2020, pp. 4127-4136+4144.
8. Mahabadi, O. K., Lisjak, A., Munjiza, A., Grasselli, G., "Y-Geo: New Combined Finite-Discrete Element Numerical Code for Geomechanical Applications". *International Journal of Geomechanics*, 12(6), 2012, pp. 676-688.
9. Sarfarazi, V., Asgari, K., Naderi, A. A., "Relationship between point load index and mode II fracture toughness of granite". *Computers and Concrete,* 28(1), 2021, pp. 25-37.
10. Haeri, H., Sarfarazi, V., Zhu, Z. M., Nejati, H. R., "Numerical simulations of fracture shear test in anisotropy rocks with bedding layers". *Adv Concr Constr,* 7(4), 2019, pp. 241-247.
11. Kirmaci, A., Erkayaoglu, M., "Thermographic analysis of failure for different rock types under uniaxial loading". *Geomech Eng,* 23(6), 2020, pp. 503-512.
12. Zheng, F., Zhuang, X. Y., Zheng, H., Jiao, Y. Y., Rabczuk, T., "Discontinuous deformation analysis with distributed bond for the modelling of rock deformation and failure". *Computers and Geotechnics,* 139, 2021, pp. 1-15.
13. Van Eldert, J., Funehag, J., Schunnesson, H., Saiang. D., "Drill Monitoring for Rock Mass Grouting: Case Study at the Stockholm Bypass". *Rock Mechanics and Rock Engineering,* 54(2), 2021, pp. 501-511.
14. Wang, C., Li, J., Wang, C., Xiong, Z. Q., Hu, M. G., Zhang, P. L., Lei. B. B., Xiong, H. W., "Damage and failure mechanism of concentric perforated granite under static pressure after alternating action of high temperature and water at different temperatures". *Engineering Fracture Mechanics,* 253, 2021, pp. 1-16.
15. Jorne, F., Henriques, F. M. A., "Evaluation of the grout injectability and types of resistance to grout flow". *Construction and Building Materials,* 122, 2016, pp. 171-183.
16. Milad, Sangsefidi, Javad, Akbardoost, Ali, Reza, Zhaleh, "Assessment of mode I fracture of rock-type sharp V-notched samples considering the size effect". *Theoretical and Applied Fracture Mechanics,* 116, 2021, pp. 1-8.
17. Chen, M. L., Jing, H. W., Ma, X. J., Su, H. J., Du, M. R., Zhu, T. T., "Fracture evolution characteristics of sandstone containing double fissures and a single circular hole under uniaxial compression". *International Journal of Mining Science and Technology,* 27(3), 2017, pp. 499-505.
18. Bi, X. F., Wang, W. C., Zhu, G. F., Liu, X. L., "Study of mechanical behavior of salt rock with prefabricated fissures under different confining pressures". *Arabian Journal of Geosciences,* 14(9), 2021, pp. 1-11.
19. Huang, Y. H., Yang, S. Q., Tian, W. L., Zeng, W., Yu, L. Y., "An experimental study on fracture mechanical behavior of rock-like materials containing two unparallel fissures under uniaxial compression". *Acta Mechanica Sinica,* 32(3), 2016, pp. 442-455.
20. Zhou, T., Zhu, J. B., Xie, H. P., "Mechanical and Volumetric Fracturing Behaviour of Three-Dimensional Printing Rock-like Samples Under Dynamic Loading". *Rock Mechanics and Rock Engineering,* 53(6), 2020, pp. 2855-2864.
21. Le, H. L., Sun, S. R., Kulatilake, Phsw, Wei, J. H., "Effect of Grout on Mechanical Properties and Cracking Behavior of Rock-Like Specimens Containing a Single Flaw under Uniaxial Compression". *International Journal of Geomechanics,* 18(10), 2018, pp. 1-16.
22. Chava. S., Namilae, S., Al-Haik, M., "Residual stress reduction during composite manufacturing through cure modification: In situ analysis". *Journal of Composite Materials,* 56(6), 2022, pp. 975-988.
23. Li, Z., Liu, J. C., Xu, R. C., Liu, H. X., Shi, W. H., "Study of grouting effectiveness based on shear strength evaluation with experimental and numerical approaches". *Acta Geotechnica,* 16(12), 2021, pp. 3991-4005.
24. Wang, Y., Xiong, Z. Q., Wang, C., Su, C. D., Li, X. F., "Research on the Reasonable Grouting Strength of Rock-Like Samples in Different Strengths". *Materials,* 13(14), 2020, pp. 1-15.
25. Alejano, L. R., Walton, G., Gaines, S., "Residual strength of granitic rocks". *Tunnelling and Underground Space Technology,* 118, 2021, pp. 1-18.
26. Hajiabdolmajid, V., Kaiser, P., "Brittleness of rock and stability assessment in hard rock tunneling". *Underground Space Technology Incorporating Trenchless Technology Research,* 18(1), 2003, pp. 35-48.
27. Heng, S., Yang, C., Li, Z., Wang, L., Hou Z. K., "Shale brittleness estimation based on energy dissipation". *Journal of Central South University (Science and Technology)* 47(02), 2016, pp. 577-585.
28. Xie, H. P., Li, L. Y., Ju, Y., Pen, R. D., Yang, Y. M., "Energy analysis for damage and catastrophic failure of rocks". *Science China-Technological Sciences,* 54, 2011, pp. 199-209.
29. He, M. M., Pang, F., Wang, H. T., Zhu, J. W., Chen, Y. S., "Energy Dissipation-Based Method for Strength Determination of Rock under Uniaxial Compression". *Shock and Vibration,* 3, 2020, pp. 1-13.
30. Zhang, M. W., Meng, Q. B., Liu, S. D., "Energy Evolution Characteristics and Distribution Laws of Rock Materials under Triaxial Cyclic Loading and Unloading Compression". *Advances in Materials Science and Engineering,* 2017, pp. 1-16.